IEEE Access
Multidisciplinary | Rapid Review | Open Access Journal

Received December 20, 2021, accepted January 19, 2022, date of publication January 31, 2022, date of current version February 11, 2022.

Digital Object Identifier 10.1109/ACCESS.2022.3148211

Magnetic Field and Temperature Dual-Parameter Sensor Based on Nonadiabatic Tapered Microfiber Cascaded With FBG

YUXIU ZHANG[1], SHENGLI PU[1,2], YONGXI LI[1], ZIJIAN HAO[1], DIHUI LI[1], SHAOKANG YAN[1], MIN YUAN[1], AND CHENCHENG ZHANG[1]

[1]College of Science, University of Shanghai for Science and Technology, Shanghai 200093, China
[2]Shanghai Key Laboratory of Modern Optical System, University of Shanghai for Science and Technology, Shanghai 200093, China

Corresponding author: Shengli Pu (shlpu@usst.edu.cn)

This work was supported in part by the National Natural Science Foundation of China under Grant 62075130 and Grant 61675132, in part by the Shanghai "Shuguang Program" under Grant 201529, and in part by the Shanghai Talent Development Fund under Grant 201529.

ABSTRACT A kind of dual-parameter sensor based on magnetic-fluid-coated nonadiabatic tapered microfiber (NTF) cascaded with fiber Bragg grating (FBG) is proposed and experimentally demonstrated. Simultaneous measurement of magnetic field and temperature is realized by monitoring the variation of NTF interference spectrum and FBG characteristic dip. In the magnetic field range of 0-18 mT, the highest magnetic field sensitivity can reach 1.159 nm/mT. The maximum temperature sensitivity is up to −1.737 nm/°C in the temperature range of 25-50 °C. The proposed magnetic-fluid-coated NTF interferometer cascaded with FBG will find extensive application prospect due to its high sensitivity, easy fabrication, compactness, strong robustness, and low cost.

INDEX TERMS Nonadiabatic tapered fiber, FBG, magnetic fluid, magnetic field measurement, temperature measurement.

I. INTRODUCTION

Compared with the traditional singlemode-multimode-singlemode (SMS) structure, tapered microfiber is an effective way to reduce fiber diameter and increase the interaction between evanescent field and the surrounding environment, which can lead to increase in sensitivity [1]–[3]. In addition, the structure is compact and easy to manufacture. The sensing characteristics of tapered microfiber have been extensively studied in various fields including current sensing [4], water pollution monitoring [5], optoacoustic emitter [6], humidity measurement [7], refractive index measurement [8]–[10], temperature sensing [11]–[13], and magnetic field sensing [14], [15]. Tapered microfiber can be divided into adiabatic tapered microfiber (ATF) and nonadiabatic tapered microfiber (NTF)[16], [17]. NTF has a large taper angle variation and the cladding mode excited in the cone region is coupled with the core mode. But for ATF, the taper angle changes very small, and the coupling does not occur in the cone region.

The associate editor coordinating the review of this manuscript and approving it for publication was Sukhdev Roy.

Magnetic field sensors have been widely used in many scientific and industrial applications, including biomedical detection, aviation industry, space and geophysical research. Several fiber optic magnetic field sensors based on different sensing technologies have been reported, including Faraday effect [18], [19], and magnetostrictive materials [20]–[24]. Nevertheless, in certain cases, the integration process of this type of material with the optical fiber is not easy. In recent years, sensors based on magnetic fluid (MF) have been widely studied. MF is a kind of stable colloidal solution, which is composed of nanometer magnetic solid particles, carrier solution and surfactant. It not only has the fluidity of liquid but also has the magnetic properties of magnetic materials. It is widely used for designing various new-fashioned fiber-optic magnetic field sensors. The employed structures include tapered photonic crystal fiber [25], side-polished fiber [26], fiber F-P cavity [27], fiber Bragg grating (FBG) [28]–[31], and long period gratings (LPGs) [32]–[35]. Although these structures are common and easy to use in practice, they are complicated and expensive to make. However, NTF is easy to manufacture and low-cost. Besides, magnetic field sensor based on NTF can significantly improve

the sensitivity. In 2014, Layeghi has already proposed a magnetic field sensor based on NTF [14], but the magnetic field sensitivity is relatively low. In this work, the magnetic field sensitivity is improved by about 16 times after parameter optimization.

FBG is usually employed to realize multiphysical measurement sensor, such as strain-temperature sensor, refractive index-temperature sensor, magnetic field-temperature sensor. Due to the refractive index of MF is affected by magnetic field and temperature, the temperature cross-sensitivity of fiber-optic magnetic field sensor based on MF cannot be ignored. In most cases, magnetic field and temperature should be measured simultaneously. In 2014, a novel fiber-optic F-P magnetic field sensor was proposed by Zhao et al [36]. In 2020, a photonic crystal fiber cascaded grating structure was proposed by Wang et al [37]. The temperature cross-sensitivity of the two sensors can be well eliminated, but they are difficult to fabricate.

In this work, a composite magnetic field sensor based on MF-coated NTF cascaded with FBG is proposed. The FBG is insensitive to magnetic field, which is used to solve the problem of temperature cross-sensitivity. Meanwhile, the NTF structure enables the high magnetic field and temperature sensitivity.

II. SENSING PRINCIPLE

The sensing principle of the NTF structure is based on the optical path difference between the core mode and cladding mode. As shown in Figure 1, the incident light reaches the first descending cone region and excites cladding mode at the uniform waist region. At the ascending cone region, the cladding mode is recoupled to the fiber core. The structure can be considered as a mode interferometer. Because the propagation constants of core mode and cladding mode are different, the comb spectrum is generated at the output. The output intensity of the interferometer can be expressed as [38], [39]

$$I = I_{core} + I_{clad} + 2\sqrt{I_{core} I_{clad}} \cos(\Delta\Phi), \tag{1}$$

where I_{core} and I_{clad} are the intensities of the fundamental core mode and cladding mode, respectively. $\Delta\Phi$ represents the phase difference between the core mode and cladding mode, which can be expressed as

$$\Delta\Phi = \frac{2\pi}{\lambda} \Delta n_{eff} L, \tag{2}$$

where λ represents the wavelength of the incident light, and L is the uniform waist length. Δn_{eff} is the effective refractive index difference between the core mode and cladding mode, which is given as $\Delta n_{eff} = n_{eff}^{core} - n_{eff}^{clad}$ ($\Delta n_{eff} > 0$). n_{eff}^{core} and n_{eff}^{clad} are the effective refractive indices of the core mode and cladding mode, respectively. According to (1), when $\Delta\Phi$ is an odd multiple of π, the output light intensity is minimum. In equation (2), the wavelength of the m-order interference valley λ_m can be expressed as

$$\lambda_m = \frac{2\Delta n_{eff} L}{2m+1}. \tag{3}$$

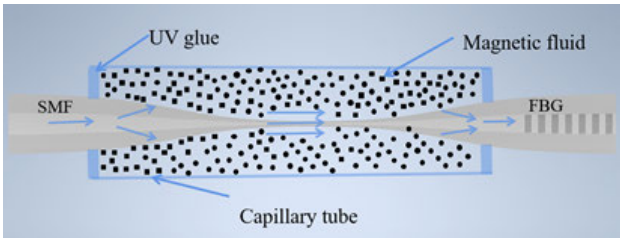

FIGURE 1. Schematic of the magnetic-fluid-coated nonadiabatic tapered microfiber cascaded with FBG structure.

When the external magnetic field intensity changes, the refractive index of MF also changes [40]. When the refractive index of MF increases, n_{eff}^{core} and n_{eff}^{clad} also increase, but the increase of n_{eff}^{core} is much larger than that of n_{eff}^{clad} [12]. Therefore, the effective refractive index difference between the two modes Δn_{eff} increases by δn_{eff} ($\delta n_{eff} > 0$), which results in the long wavelength shift for the interference spectrum. According to (3), the wavelength shift of the m-order interference valley is given as [41]:

$$\begin{aligned} \Delta\lambda_{\mathrm{m}} &= \lambda_m' - \lambda_{\mathrm{m}} \\ &= \frac{2(\Delta n_{efff} + \delta n_{eff})L}{(2\mathrm{m}+1)} - \frac{2\Delta n_{eff} L}{(2m+1)} \\ &= \frac{2\delta n_{eff} L}{(2\mathrm{m}+1)}. \end{aligned} \tag{4}$$

Similarly, when the ambient temperature changes, the refractive index of MF also changes [40], [42]. When the temperature increases, the refractive index of MF decreases, which leads to the reduction of n_{core} and n_{clad}. Therefore, the effective refractive index difference between the two modes Δn_{eff} decreases by δn_{eff} ($\delta n_{eff} > 0$), which leads to the shift of interference spectrum with temperature. According to (3), the wavelength shift of m-order interference dip can be expressed as

$$\begin{aligned} \Delta\lambda_m &= \frac{2(\Delta n_{efff} - \delta n_{eff})L}{(2\mathrm{m}+1)} - \frac{2\Delta n_{eff} L}{(2\mathrm{m}+1)} \\ &= -\frac{2\delta n_{eff} L}{(2\mathrm{m}+1)}. \end{aligned} \tag{5}$$

When the MF-coated NTF is cascaded with a FBG, the Bragg transmission valley is expressed as [43]

$$\lambda_{FBG} = 2n_{eff}^{core} \Lambda, \tag{6}$$

where Λ represents the period of FBG. n_{eff}^{core} is independent of the external environment. Therefore, the transmission spectrum of FBG is insensitive to magnetic field change. However, the change of temperature will affect the transmission, the Bragg wavelength shift caused by temperature can be expressed as

$$\begin{aligned} \Delta\lambda_{FBG} &= \lambda_{FBG}(\alpha_{th} + \zeta) \cdot \Delta T \\ &= K_{T,FBG} \Delta T, \end{aligned} \tag{7}$$

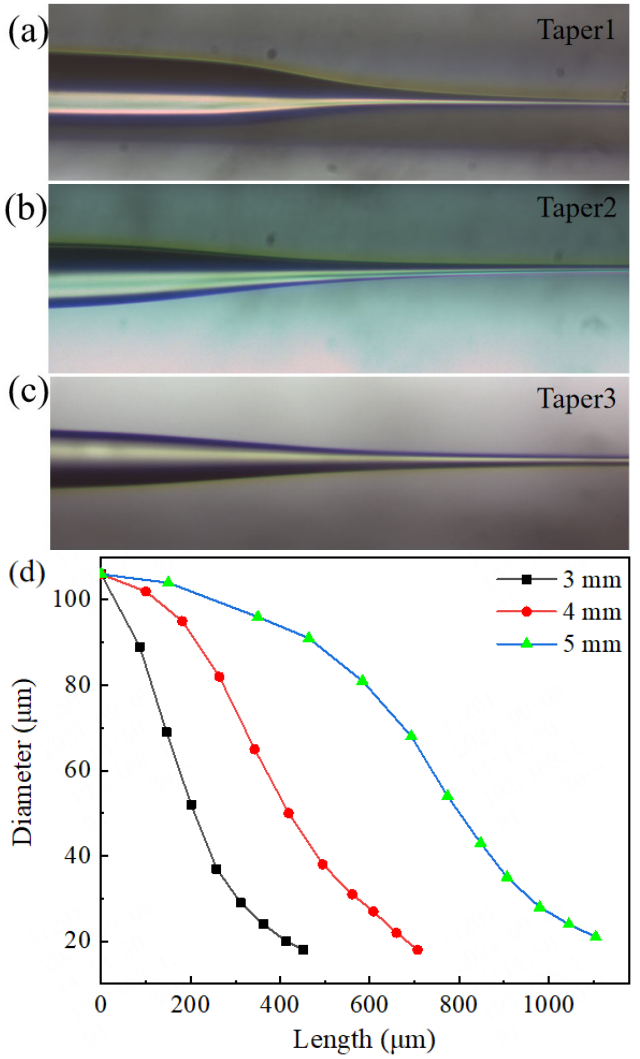

FIGURE 2. Micrographs of Taper 1 (a), Taper 2 (b), and Taper 3 (c). Profiles of the tapering regions (d).

where $\Delta\lambda_{FBG}$ is the wavelength shift, $\alpha_{\text{th}} = 0.55 \times 10^{-6}/°\text{C}$ and $\zeta = 8.0 \times 10^{-6}/°\text{C}$ are respectively the thermal expansion coefficient and thermo-optical coefficient of FBG, ΔT is the change of ambient temperature, $K_{T,FBG}$ is the temperature sensitivity coefficient.

Therefore, the wavelength shift of interference valley ($\Delta\lambda_1$) and FBG characteristic valley ($\Delta\lambda_2$) with the change of magnetic field and temperature can be expressed by the following sensitivity matrix

$$\begin{bmatrix} \Delta\lambda_1 \\ \Delta\lambda_2 \end{bmatrix} = \begin{bmatrix} K_{n_1} & K_{T_1} \\ K_{n_2} & K_{T_2} \end{bmatrix} \begin{bmatrix} \Delta H \\ \Delta T \end{bmatrix}, \tag{8}$$

where K_{n_1} and K_{T_1} represent the magnetic field and temperature sensitivity coefficients of the interference valley. K_{n_2} and K_{T_2} are the magnetic field and temperature sensitivity coefficients of FBG characteristic valley. Since FBG is not sensitive to magnetic field, K_{n_2} is equal to 0. ΔH and ΔT are the change of external magnetic field intensity and temperature, respectively. Through the inverse matrix of (8),

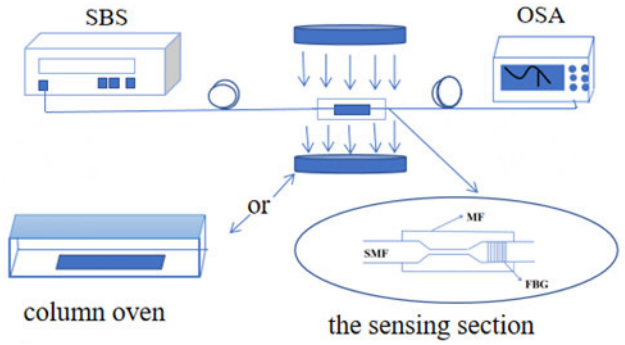

FIGURE 3. Schematic of experimental setup for measuring the magnetic field and temperature sensing properties.

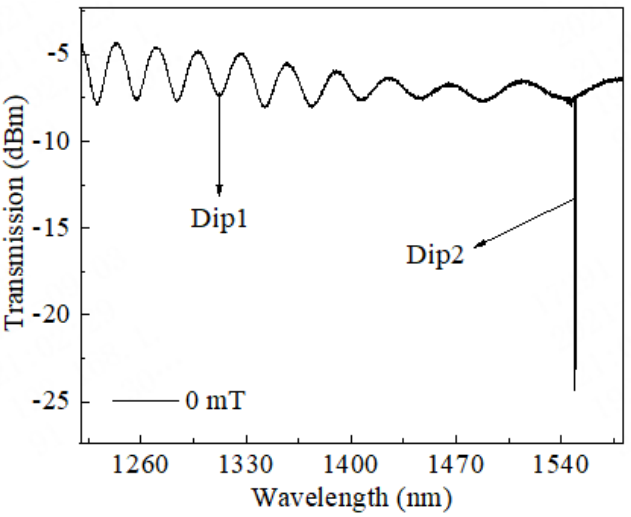

FIGURE 4. Typical transmission spectrum of the sensing structure (Taper 1 cascaded with FBG) under zero magnetic field.

simultaneous measurement of temperature and magnetic field can be realized through the following matrix

$$\begin{bmatrix} \Delta H \\ \Delta T \end{bmatrix} = \frac{1}{K_{n_1} K_{T_2}} \begin{bmatrix} K_{T_2} & -K_{T_1} \\ 0 & K_{n_1} \end{bmatrix} \begin{bmatrix} \Delta\lambda_1 \\ \Delta\lambda_2 \end{bmatrix}. \tag{9}$$

III. EXPERIMENTS

A. FABRICATION AND CHARACTERIZATION

The sensing structure consists of MF-coated NTF and FBG. The NTF is obtained by singlemode fiber taper. The core/cladding diameter of SMF is 9/125 μm. The detailed fabrication is divided into two steps: firstly, cupped fiber taper is made by discharging with the optical fiber fusion splicer (AV6471); then the cupped fiber taper is placed on the fiber-pulling machine. Hydrogen flame is employed to further taper the fiber. Finally, the NTF is obtained. Through setting different tapering parameters, such as discharge power (30 bit-100 bit), discharge time (1 sec-6 sec), and pulling speed (300 -900 $\mu m/s$), three sensing structures with different taper lengths are obtained. In order to avoid possible bending and fracture of the tapered fiber, the three structures are

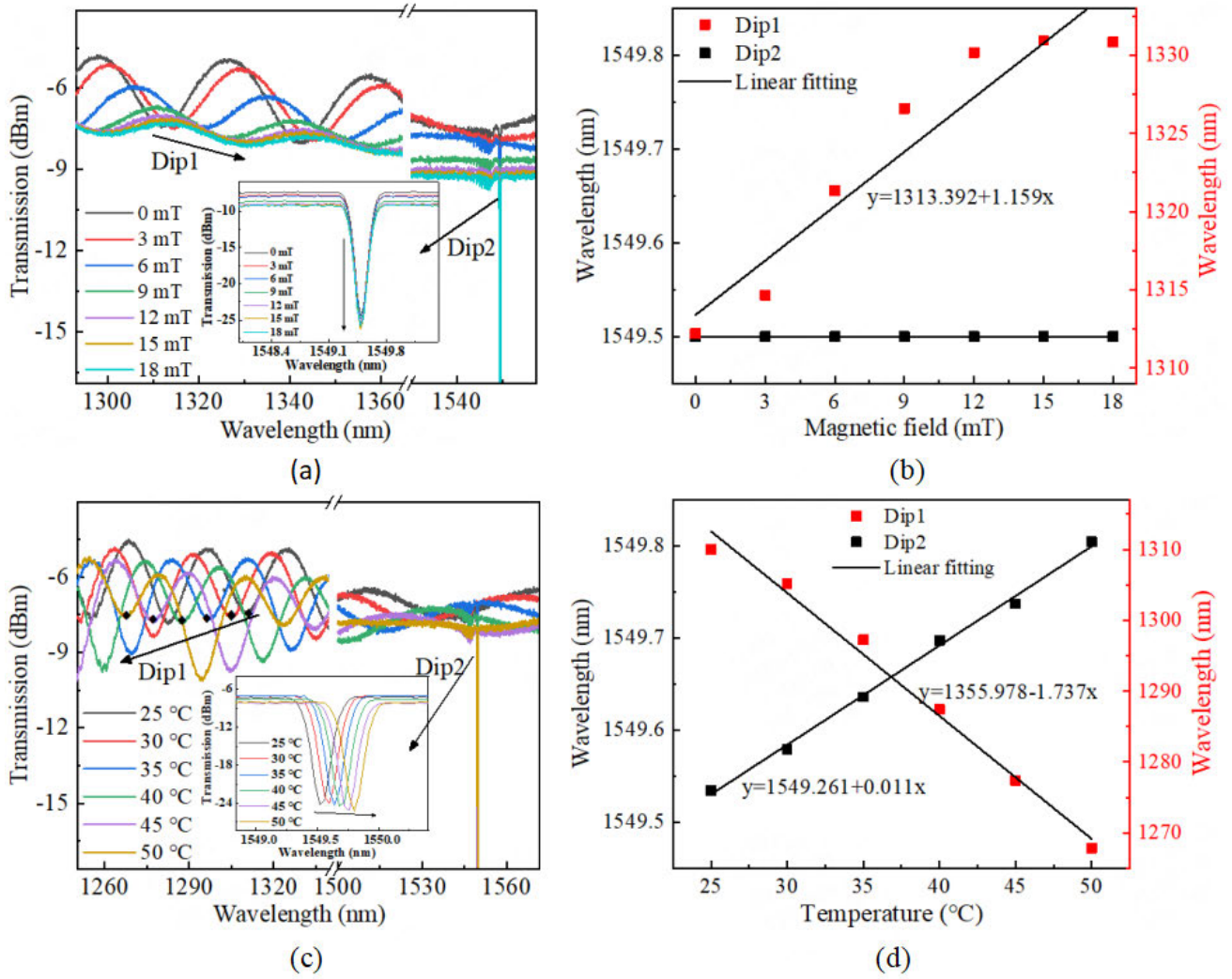

FIGURE 5. **(a)Transmission spectra of the sensing structure (Taper 1 cascaded with FBG) at different magnetic field intensities. The inset is the enlarged transmission spectra at the FBG wavelength; (b) Wavelength of Dip 1 and Dip 2 as a function of magnetic field. (c) Transmission spectra of the sensing structure (Taper 1 cascaded with FBG) at different temperatures. The inset is the enlarged transmission spectra at the FBG wavelength; (d) Wavelength of Dip 1 and Dip 2 as a function of temperature.**

first fixed in quartz groove, and then encapsulated in tube filled with MF. Both ends of the simple tube are sealed with UV glue to prevent the flowing of MF. The employed water-based MF is EMG605, which is provided by Ferrotec Co., LTD. The MF is diluted with distilled water. The refractive index of the final MF is 1.339, which is measured with a refractometer (A670, Hanon, China). Then, the packaged NTF is cascaded with a FBG, which is provided by Henan Minghai Optoelectronic Technology Co., LTD. The central wavelength of the FBG is 1550 nm, and the grating length is 10 mm.

The waist diameter of the three NTFs was kept at 5 μm and the interference arm lengths were 3 mm, 4 mm and 5 mm, respectively. The corresponding NTFs are referred as Taper 1, Taper 2 and Taper 3. Their micrographs are shown in Figure 2(a)-2(c). The profiles of the corresponding tapering regions are shown in Figure 2(d), which indicates that the profile for Taper 1 is steepest. The steepness of the profile influences the transmission of the sensing structure greatly.

B. EXPERIMENTAL DETAILS

The experimental setup for measuring the magnetic field and temperature sensing properties of the as-fabricated devices is shown in Figure 3. The sensing structure is connected to the super continuous broadband light source (SBS, Wuhan Yangtze Soton Laser Co., Ltd., Wuhan) and the optical spectral analyzer (OSA, Yokogawa AQ6370C). The light emitted from SBS has a wavelength range of 700-1700 nm. The resolution of OSA is set at 0.2 nm. The direction of magnetic field is perpendicular to the optical fiber axis. The intensity of magnetic field is adjusted by changing the supply current. The equipment is provided by East Changing Co., Ltd. The sensing area is placed in the magnetic field. The intensity of magnetic field is calibrated with a Gauss meter.

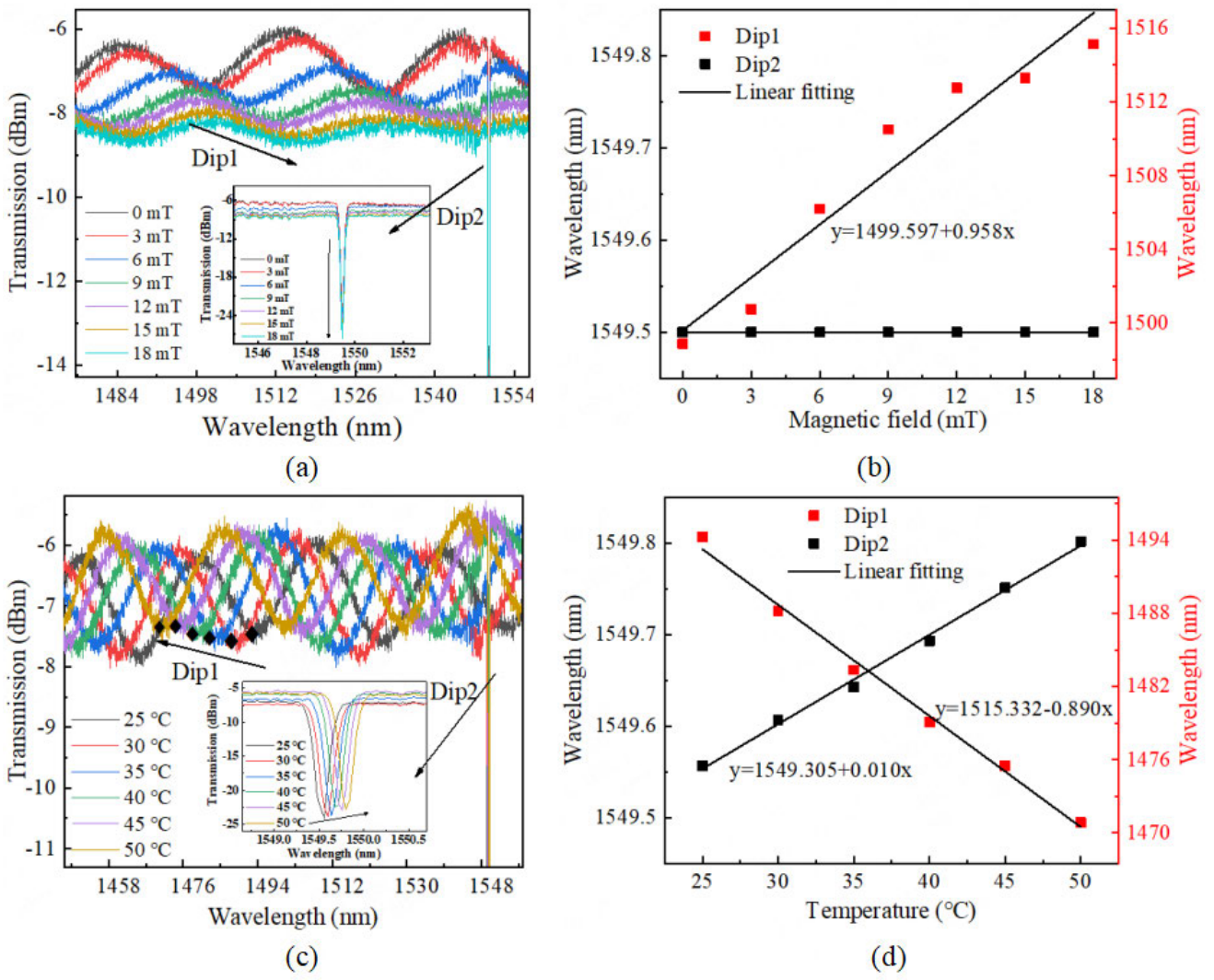

FIGURE 6. (a) Transmission spectra of the sensing structure (Taper 2 cascaded with FBG) at different magnetic field intensities. The inset is the enlarged transmission spectra at FBG wavelength. (b) Wavelength of Dip 1 and Dip 2 as a function of magnetic field. (c) Transmission spectra of the sensing structure (Taper 2 cascaded with FBG) at different temperatures. The inset is the enlarged transmission spectra at the FBG wavelength. (d) Wavelength of Dip 1 and Dip 2 as a function of temperature.

For temperature test, the sensing device is placed in a columnar temperature control oven (LCO 102 LONG, ECOM Ltd., Czech Republic). The temperature adjustment resolution is 0.1 °C.

IV. RESULTS AND DISCUSSION

The typical transmission spectrum of the sensing structure (Taper 1 cascaded with FBG) under zero magnetic field is shown in Figure 4. The maximum wavelength shift sensitivity occurs for the dip at around 1311 nm (referred as Dip 1), which is selected for the subsequent analysis. The dip at round 1550 nm (referred as Dip 2) has a large extinction ratio, which is the FBG characteristic dip.

The transmission spectra of Taper 1 cascaded with FBG under different magnetic field intensities are shown in Fig. 5(a). The mode interference dip (viz. Dip 1) drifts towards long wavelength with the magnetic field and the maximum drift reaches 18.647 nm. While the FBG dip (viz. Dip 2) is insensitive to magnetic field. When the external magnetic field intensity increases from 0 mT to18 mT, the refractive index of MF increases. The obtained experimental results are consistent with the aforementioned theoretical analysis. The magnetization saturation of MF used in the experiment is 20 mT. So, when the magnetic field continues to grow, the wavelength shift is not obvious at higher magnetic field. Fig. 5(b) explicitly depicts the relationship between dip wavelength and magnetic field intensity. After linear fitting, the magnetic field sensitivity is obtained to be 1.159 nm/mT.

Fig. 5(c) is the transmission spectra of the sensing structure (Taper 1 cascaded with FBG) at different temperatures. It can be found that Dip 1 drifts towards short wavelength with temperature, while Dip 2 drifts towards long wavelength with temperature. As the temperature increases, the refractive index of MF decreases, which is contrary to the

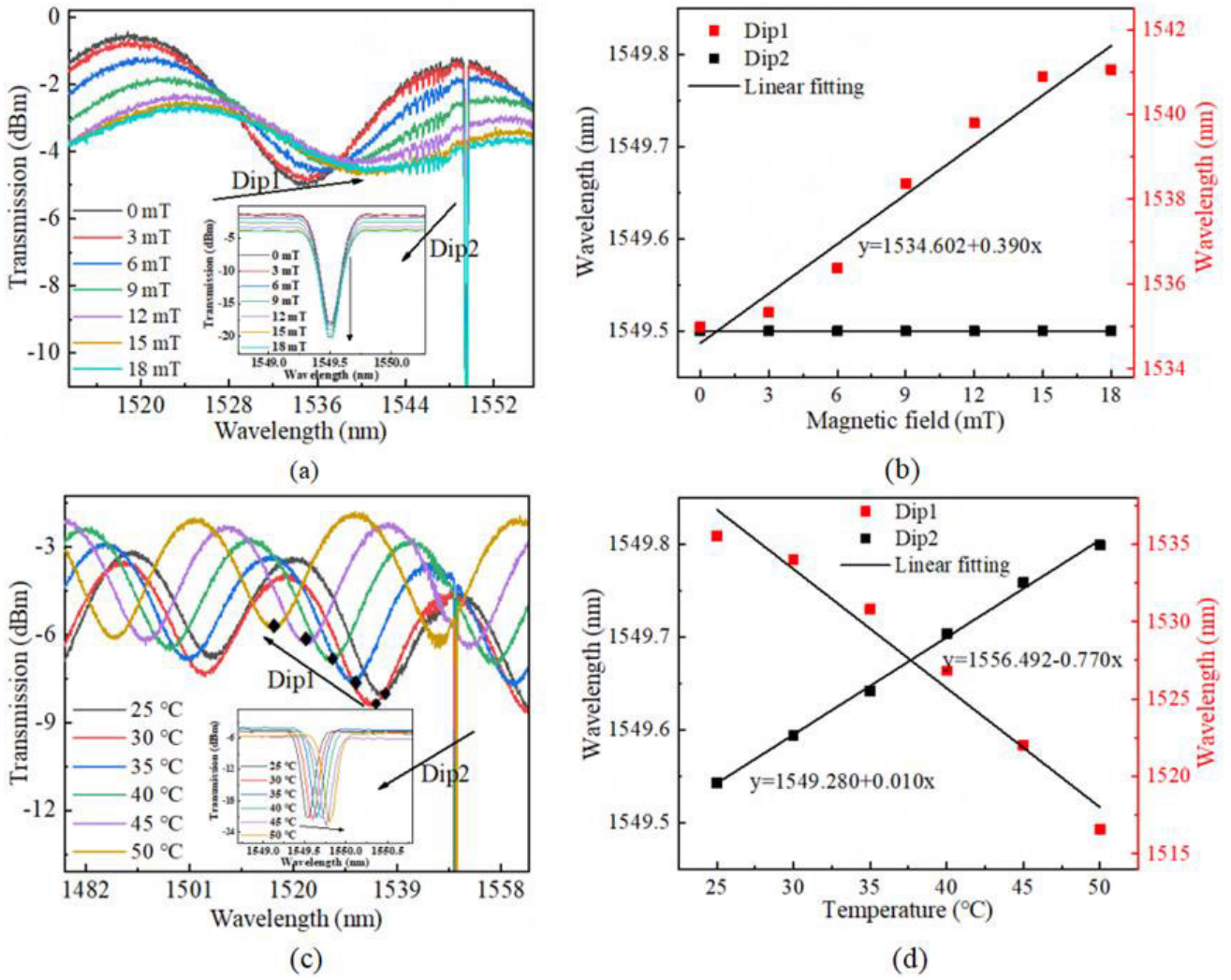

FIGURE 7. (a) Transmission spectra of the sensing structure (Taper 3 cascaded with FBG) at different magnetic field intensities. The inset is the enlarged transmission spectra at the FBG wavelength. (b) Wavelength of Dip 1 and Dip 2 as a function of magnetic field. (c) Transmission spectra of the sensing structure (Taper 3 cascaded with FBG) at different temperatures. The inset is the enlarged transmission spectra at FBG wavelength. (d) Wavelength of Dip 1 and Dip 2 as a function of temperature.

case for magnetic field increase [40]. The obtained experimental results are also consistent with the aforementioned theoretical analysis. Fig. 5 (d) explicitly gives the shift of Dip 1 and Dip 2 with temperature. The sensitivities of Dip 1 and Dip 2 are −1.737 nm/°C and 0.011 nm/°C, respectively. Higher temperature range can be obtained through further optimizing the structure and material parameters [11], [12].

Similarly, experimental results for Taper 2 cascaded with FBG are obtained and plotted in Figure 6, which shows that there are fluctuations for the transmission spectra. Thus, the wavelength corresponding to Dip 1 is obtained by smoothing the original spectrum. The magnetic sensitivity of Dip 1 is 0.958 nm/mT. The temperature sensitivities of Dip 1 and Dip 2 are −0.890 nm/°C and 0.010 nm/°C, respectively.

Finally, the experimental results for Taper 3 cascaded with FBG are shown in Fig. 7. The magnetic field and temperature sensitivities of Dip 1 are 0.390 nm/mT and −0.770 nm/°C, respectively. The temperature sensitivity of Dip 2 is 0.010 nm/°C.

TABLE 1. Maximum sensitivities of as-fabricated three sensing structures.

Sensing Structure	Magnetic Field Sensitivity (nm/mT)	Temperature Sensitivity (nm/℃)
Taper1+FBG	1.159	-1.737
Taper2+FBG	0.958	-0.890
Taper3+FBG	0.390	-0.770

To be clear, Table 1 summarizes the maximum sensitivities of the as-fabricated three sensing structures. It can be seen from Table 1 that the magnetic field and temperature sensitivities of Taper 1 cascaded with FBG are higher than those of the other two. For the three tapers, their smallest

TABLE 2. Sensing performance of various dual-parameter measurement structure.

Structures	Detecting Range	Magnetic Field Sensitivity	Temperature Sensitivity	Published Year	Reference
FP-FBG	0-60 mT	0.400 nm/mT	0.020 nm/℃	2014	[36]
SMS	0-13 mT	0.659 nm/mT	-0.042 nm/℃	2015	[2]
No-core Fiber	2-14 mT	0.074 nm/mT	-0.247 nm/°C	2016	[46]
D-shaped PCF	0-27 mT	2.10 nm/mT	-1.250 nm/°C	2019	[44]
NCF-ECSF	0-14 mT	0.713 nm/mT	0.305 nm/°C	2019	[45]
PCF-FBG	0-10 mT	0.925 nm/mT	0.123 nm/°C	2020	[37]
MZI-FBG	0-25 mT	0.408 nm/mT	-0.363 nm/°C	2019	[47]
NTF-FBG	0-18 mT	1.159 nm/mT	-1.737 nm/°C	/	This work

waist diameters are the same (i.e. 5 μm), but their steepness for the tapering region becomes smaller from Taper 1 to Taper 3. Theoretically, the shift of wavelength is greater for the structure with longer interference arm (see (4) and (5)) at the same conditions. But the experimental results indicate that the structure with shorter interreference arm length has a higher sensitivity. Thus, it can be concluded that the steepness has a greater influence on the sensitivity. The steeper the taper is, the greater their sensitivity will be.

For Taper 1 cascaded with FBG, the magnetic field and temperature can be obtained through the following matrix [Eq. (10) below]. In this way, the problem of temperature cross-sensitivity can be solved.

$$\begin{bmatrix} \Delta H \\ \Delta T \end{bmatrix} = \frac{1}{0.013} \begin{bmatrix} 0.011 & 1.737 \\ 0 & 1.159 \end{bmatrix} \begin{bmatrix} \Delta\lambda_1 \\ \Delta\lambda_2 \end{bmatrix}. \quad (10)$$

For comparison, Table 2 lists the sensing performance of various dual-parameter measurement structures. Among these structures, the magnetic field sensitivities mentioned in Refs. [37], [44] and [45] are relatively high, but they have high fabrication cost. Comparing with the structures reported in Refs. [2], [36], [46] and [47], the structure proposed in this work has a higher sensitivity for both magnetic field and temperature measurement and the fabrication cost is low.

V. CONCLUSION

In conclusion, a kind of optical microfiber sensor for simultaneously measuring magnetic field and temperature is proposed. The experimental results show that the steepness of the NTF has a greater influence on the sensitivity. The maximum magnetic field and temperature sensitivities are obtained to be 1.159 nm/mT in the magnetic field range of 0-18 mT and −1.737 nm/°C in the temperature range of 25-50 °C, respectively. Furthermore, the sensitivity can be improved by increasing the steepness when the taper radius is fixed. The advantages of the proposed sensors are simple in structure, low-cost and easy fabrication. The problem of temperature crosstalk can be overcome effectively by using the sensitivity matrix.

REFERENCES

[1] L. Li, Q. Han, Y. Chen, T. Liu, and R. Zhang, "An all-fiber optic current sensor based on ferrofluids and multimode interference," *IEEE Sensors J.*, vol. 14, no. 6, pp. 1749–1753, Jun. 2014.

[2] L. Luo, S. Pu, S. Dong, and J. Tang, "Fiber-optic magnetic field sensor using magnetic fluid as the cladding," *Sens. Actuators A, Phys.*, vol. 236, pp. 67–72, Dec. 2015.

[3] Y. Wang, Z.-R. Tong, W.-H. Zhang, P.-P. Luan, Y. Zhao, and L.-F. Xue, "Research on optical fiber magnetic field sensors based on multi-mode fiber and spherical structure," *Optoelectron. Lett.*, vol. 13, no. 1, pp. 16–20, Jan. 2017.

[4] M. Luo, Q. Yang, L. Huang, and F. Dong, "Non-contact current sensor based on micro-ring resonator," *Acta Optica Sinica*, vol. 41, no. 12, 2021, Art. no. 1228001.

[5] S. Wang, L. Zu, Y. Miao, C. Fei, H. Zhang, B. Li, K. Zhang, and F. Liu, "Simultaneous measurement of the BOD concentration and temperature based on a tapered microfiber for water pollution monitoring," *Appl. Opt.*, vol. 59, no. 24, pp. 7364–7370, 2020.

[6] L. Shi, Y. Jiang, F. R. Fernandez, G. Chen, L. Lan, H.-Y. Man, J. A. White, J.-X. Cheng, and C. Yang, "Non-genetic photoacoustic stimulation of single neurons by a tapered fiber optoacoustic emitter," *Light, Sci. Appl.*, vol. 10, no. 1, p. 143, Jul. 2021.

[7] L. Chen, B. Liu, J. Liu, J. Yuan, H. P. Chan, T. Wu, M. Wang, S.-P. Wan, X.-D. He, and Q. Wu, "U-shape panda polarization-maintaining microfiber sensor coated with graphene oxide for relative humidity measurement," *J. Lightw. Technol.*, vol. 39, no. 19, pp. 6308–6314, Oct. 15, 2021.

[8] W. B. Ji, H. H. Liu, S. C. Tjin, K. K. Chow, and A. Lim, "Ultrahigh sensitivity refractive index sensor based on optical microfiber," *IEEE Photon. Technol. Lett.*, vol. 24, no. 20, pp. 1872–1874, Oct. 15, 2012.

[9] Q. Wang, W. Wei, M. Guo, and Y. Zhao, "Optimization of cascaded fiber tapered Mach–Zehnder interferometer and refractive index sensing technology," *Sens. Actuators B, Chem.*, vol. 222, pp. 159–165, Jan. 2016.

[10] S. Li and Y. Zhao, "A Mach–Zehnder interferometer based on tapered dual side hole fiber for refractive index sensing," *Opt. Fiber Technol.*, vol. 45, pp. 267–270, Nov. 2018.

[11] M. Z. Muhammad, A. A. Jasim, H. Ahmad, H. Arof, and S. W. Harun, "Non-adiabatic silica microfiber for strain and temperature sensors," *Sens. Actuators A, Phys.*, vol. 192, pp. 130–132, Apr. 2013.

[12] T. Zhou, Y.-N. Zhang, B. Han, A. Zhang, and D. Fu, "Low cost non-adiabatic tapered fiber for high-sensitive temperature sensing," *Opt. Fiber Technol.*, vol. 45, pp. 53–57, Nov. 2018.

[13] J. Li, Z. Li, J. Yang, Y. Zhang, and C. Ren, "High sensitivity temperature probe based on elliptical microfiber knot ring," *Results Phys.*, vol. 16, Mar. 2020, Art. no. 102953.

[14] A. Layegh, H. Latif, and O. Frazao, "Magnetic field sensor based on nonadiabatic tapered optical fiber with magnetic fluid," *IEEE Photon. Technol. Lett.*, vol. 26, no. 19, pp. 1904–1907, Oct. 1, 2014.

[15] L. Mao, S. Pu, D. Su, Z. Wang, X. Zeng, and M. Lahoubi, "Magnetic field sensor based on cascaded microfiber coupler with magnetic fluid," *J. Appl. Phys.*, vol. 120, no. 9, Sep. 2016, Art. no. 093102.

[16] R. J. Black, S. Lacroix, F. Gonthier, and J. D. Love, "Tapered single-mode fibres and devices—Part 2: Experimental and theoretical quantification," *IEEE Proc. J. Optoelectron.*, vol. 138, no. 5, pp. 355–364, Oct. 1991.

[17] M. I. Zibaii, H. Latifi, M. Karami, M. Gholami, S. M. Hosseini, and M. H. Ghezelayagh, "Non-adiabatic tapered optical fiber sensor for measuring the interaction between α-amino acids in aqueous carbohydrate solution," *Meas. Sci. Technol.*, vol. 21, no. 10, Oct. 2010, Art. no. 105801.

[18] L. Sun, S. Jiang, and J. R. Marciante, "All-fiber optical magnetic-field sensor based on Faraday rotation in highly terbium-doped fiber," *Opt. Exp.*, vol. 18, no. 6, pp. 5407–5412, 2010.

[19] S. Wang, C. Sun, L. Du, C. Yao, and Y. Yang, "Reciprocity of Faraday effect in ferrofluid: Comparison with magneto-optical glass," *Optik*, vol. 123, no. 6, pp. 553–558, Mar. 2012.

[20] G. Ding, S. Zhang, H. Cao, B. Gao, and B. Zhang, "Flux density measurement of radial magnetic bearing with a rotating rotor based on fiber Bragg grating-giant magnetostrictive material sensors," *Appl. Opt.*, vol. 56, no. 17, pp. 4975–4981, 2017.

[21] M. Rui, Z. Wen-Tao, W. Zhao-Gang, H. Wen-Zhu, and L. Fang, "Magnetic sensor based on Terfenol-D materials and fiber Bragg grating Fabry–Pérot cavity," *Acta Photonica Sinica*, vol. 47, no. 3, 2018, Art. no. 306006.

[22] B. Zhan, T. Ning, L. Pei, J. Li, L. Liu, X. Gao, J. Xu, J. Zheng, J. Wang, and B. Ai, "Terfenol-D based magnetic field sensor with temperature independence incorporating dual fiber Bragg gratings structure," *IEEE Access*, vol. 9, pp. 32713–32720, 2021.

[23] C. Liu, T. Shen, H.-B. Wu, Y. Feng, and J.-J. Chen, "Applications of magneto-strictive, magneto-optical, magnetic fluid materials in optical fiber current sensors and optical fiber magnetic field sensors: A review," *Opt. Fiber Technol.*, vol. 65, Sep. 2021, Art. no. 102634.

[24] H. Liu, S. W. Or, and H. Y. Tam, "Magnetostrictive composite–fiber Bragg grating (MC–FBG) magnetic field sensor," *Sens. Actuators A, Phys.*, vol. 173, no. 1, pp. 122–126, Jan. 2012.

[25] Y. Zhao, D. Wu, and R.-Q. Lv, "Magnetic field sensor based on photonic crystal fiber taper coated with ferrofluid," *IEEE Photon. Technol. Lett.*, vol. 27, no. 1, pp. 26–29, Jan. 1, 2015.

[26] Y. Li, S. Pu, Y. Zhao, R. Zhang, Z. Jia, J. Yao, Z. Hao, Z. Han, D. Li, and X. Li, "All-fiber-optic vector magnetic field sensor based on side-polished fiber and magnetic fluid," *Opt. Exp.*, vol. 27, no. 24, pp. 35182–35188, Nov. 2019.

[27] F. Shi, Y. Luo, J. Che, Z. Ren, and B. Peng, "Optical fiber F–P magnetic field sensor based on magnetostrictive effect of magnetic fluid," *Opt. Fiber Technol.*, vol. 43, pp. 35–40, Jul. 2018.

[28] A. Candiani, M. Konstantaki, W. Margulis, and S. Pissadakis, "A spectrally tunable microstructured optical fibre Bragg grating utilizing an infiltrated ferrofluid," *Opt. Exp.*, vol. 18, no. 24, pp. 24654–24660, Nov. 2010.

[29] W. Lin, Y. Miao, H. Zhang, B. Liu, Y. Liu, B. Song, and J. Wu, "Two-dimensional magnetic field vector sensor based on tilted fiber Bragg grating and magnetic fluid," *J. Lightw. Technol.*, vol. 31, no. 15, pp. 2599–2605, Aug. 15, 2013.

[30] W. Bao, X. Qiao, Q. Rong, and F. Chen, "Fiber-optic vector magnetometer based on magnetic fluid and fiber Bragg grating written on a multi-clad fiber," *IEEE Sensors J.*, vol. 18, no. 18, pp. 7486–7491, Sep. 2018.

[31] P. Li, H. Yan, Z. Xie, Y. Li, and X. Zhao, "An intensity-modulated and large bandwidth magnetic field sensor based on a tapered fiber Bragg grating," *Opt. Laser Technol.*, vol. 125, May 2020, Art. no. 105996.

[32] T. Liu, X. Chen, Z. Di, J. Zhang, X. Li, and J. Chen, "Tunable magneto-optical wavelength filter of long-period fiber grating with magnetic fluids," *Appl. Phys. Lett.*, vol. 91, no. 12, 2007, Art. no. 12116.

[33] J. Luo, G. Zhang, N. Xie, T. Wang, Y. Gu, S. Gong, and C. Wang, "A magnetic sensor based on a hybrid long-period fiber grating and a magnetic fluid," *IEEE Photon. Technol. Lett.*, vol. 27, no. 9, pp. 998–1001, May 1, 2015.

[34] J. Tang, S. Pu, L. Luo, and S. Dong, "Simultaneous measurement of magnetic field and temperature based on magnetic fluid-clad long period fiber grating," *J. Eur. Opt. Soc., Rapid Publications*, vol. 10, p. 15025, May 2015.

[35] C. Jiang, Y. Liu, and C. Mou, "Polarization-maintaining fiber long-period grating based vector curvature sensor," *IEEE Photon. Technol. Lett.*, vol. 33, no. 7, pp. 358–361, Apr. 1, 2021.

[36] Y. Zhao, R.-Q. Lv, D. Wang, and Q. Wang, "Fiber optic Fabry–Pérot magnetic field sensor with temperature compensation using a fiber Bragg grating," *IEEE Trans. Instrum. Meas.*, vol. 63, no. 9, pp. 2210–2214, Sep. 2014.

[37] J. Wang, L. Pei, J. Wang, Z. Ruan, J. Zheng, J. Li, and T. Ning, "Magnetic field and temperature dual-parameter sensor based on magnetic fluid materials filled photonic crystal fiber," *Opt. Exp.*, vol. 28, no. 2, pp. 1456–1471, Jan. 2020.

[38] Y. Hu, C. Jiang, M. Zhou, and J. Liu, "High-sensitivity fiber temperature and refractive index sensing with nonadiabatic fiber taper," *J. Opt. Technol.*, vol. 85, no. 4, pp. 233–237, 2018.

[39] T. K. Yadav, R. Narayanaswamy, M. H. A. Bakar, Y. M. Kamil, and M. A. Mahdi, "Single mode tapered fiber-optic interferometer based refractive index sensor and its application to protein sensing," *Opt. Exp.*, vol. 22, no. 9, pp. 22802–22807, Sep. 2014.

[40] C. Y. Hong, H. E. Horng, and S. Y. Yang, "Tunable refractive index of magnetic fluids and its applications," *Phys. Status Solidi C*, vol. 1, no. 7, pp. 1604–1609, May 2010.

[41] M. Arjmand, H. Saghafifar, M. Alijanianzadeh, and M. Soltanolkotabi, "A sensitive tapered-fiber optic biosensor for the label-free detection of organophosphate pesticides," *Sens. Actuators B, Chem.*, vol. 249, pp. 523–532, Oct. 2017.

[42] Y. F. Chen, S. Y. Yang, W. S. Tse, H. E. Horng, C.-Y. Hong, and H. C. Yang, "Thermal effect on the field-dependent refractive index of the magnetic fluid film," *Appl. Phys. Lett.*, vol. 82, no. 20, pp. 3481–3483, May 2003.

[43] K. O. Hill and G. Meltz, "Fiber Bragg grating technology fundamentals and overview," *J. Lightw. Technol.*, vol. 15, no. 8, pp. 1263–1276, Aug. 15, 1997.

[44] Y. Ying, N. Hu, G.-Y. Si, K. Xu, N. Liu, and J.-Z. Zhao, "Magnetic field and temperature sensor based on D-shaped photonic crystal fiber," *Optik*, vol. 176, pp. 309–314, Jan. 2019.

[45] C. Sun, M. Wang, Y. Dong, S. Ye, and S. Jian, "Simultaneous measurement of magnetic field and temperature based on NCF cascaded with ECSF in fiber loop mirror," *Opt. Fiber Technol.*, vol. 48, pp. 45–49, Mar. 2019.

[46] G.-H. Su, J. Shi, D.-G. Xu, H.-W. Zhang, W. Xu, Y.-Y. Wang, J.-C. Feng, and J.-Q. Yao, "Simultaneous magnetic field and temperature measurement based on no-core fiber coated with magnetic fluid," *IEEE Sensors J.*, vol. 16, no. 23, pp. 8489–8493, Sep. 2016.

[47] R. Zhang, S. Pu, Y. Li, Y. Zhao, Z. Jia, J. Yao, and Y. Li, "Mach–Zehnder interferometer cascaded with FBG for simultaneous measurement of magnetic field and temperature," *IEEE Sensors J.*, vol. 19, no. 11, pp. 4079–4083, Jun. 2019.

YUXIU ZHANG was born in 1996. She received the B.S. degree in physics from Datong University. She is currently pursuing the master's degree with the College of Science, University of Shanghai for Science and Technology.

SHENGLI PU was born in 1978. He received the Ph.D. degree from Shanghai Jiao Tong University, in 2006. He is currently a Professor with the College of Science, University of Shanghai for Science and Technology. He is also a Visiting Associate Professor at Cornell University, from August 2012 to August 2013. He has coauthored over 130 peer-reviewed papers in *Physics* and *Optics*. His research interests include advanced photonic materials and devices, especially the novel optical properties and photonic applications of magnetic fluids/ferrofluids.

YONGXI LI was born in 1996. He received the bachelor's and master's degrees from the College of Science, University of Shanghai for Science and Technology. He is currently working in a company related with to physics.

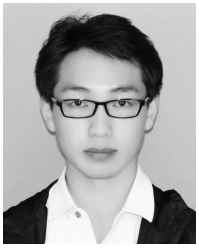

ZIJIAN HAO was born in 1996. He received the B.S. degree from the Binjiang College, Nanjing University of Information Science & Technology. He is currently pursuing the Ph.D. degree with the College of Science, University of Shanghai for Science and Technology.

DIHUI LI was born in 1994. He received the B.S. degree from the East China University of Technology and the master's degree from the College of Science, University of Shanghai for Science and Technology. He is currently working in a company related with physics.

SHAOKANG YAN was born in 1993. He received the B.S. degree from Handan University. He is currently pursuing the master's degree with the College of Science, University of Shanghai for Science and Technology.

MIN YUAN was born in 1997. She received the B.S. degree from Hubei Normal University. She is currently pursuing the master's degree with the College of Science, University of Shanghai for Science and Technology.

CHENCHENG ZHANG was born in 1995. She received the B.S. degree from the Suzhou University of Science and Technology. She is currently pursuing the master's and Ph.D. degrees with the College of Science, University of Shanghai for Science and Technology.